Microscopic description of the E0, E2 and E1 giant resonances in ^{40}Ca, ^{48}Ca and ^{56}Ni

S. Kamerdzhiev[1,2], J. Speth[1], G. Tertychny[1,2]

[1]Forschungszentrum Jülich, Institut für Kernphysik,
D-52425 Jülich, Germany

[2]Institute of Physics and Power Engineering,
249020 Obninsk, Russia

KFA-IKP(TH)-1997-04

KFA-IKP(TH)-1997-04

Microscopic description of the E0, E2 and E1 giant resonances in ^{40}Ca, ^{48}Ca and ^{56}Ni .

S. Kamerdzhiev[a,b], J.Speth[b] and G.Tertychny[a,b]

[a] *Institute of Physics and Power Engineering, 249020 Obninsk, Russia,*

[b] *Institut für Kernphysik, Forschungszentrum Jülich,*

D-52428 Jülich, Germany

Abstract

The isovector E1 as well as the isoscalar, isovector and full electromagnetic E2 and E0 strength distributions for ^{40}Ca, ^{48}Ca and ^{56}Ni have been calculated in a large energy range up to 50 MeV of excitation. The microscopic model used includes the continuum RPA, 1p1h⊗phonon configurations and ground state correlations induced by these configurations. It is shown that the latter effect gives an increase of the energy weighted sum rules of 4 - 7%. In all these nuclei the isoscalar E0 and E2 resonances are spread out over the broad energy region. We obtained a reasonable good agreement with the available experimental data including the recent ones for the isoscalar E0 resonance in ^{40}Ca. The theoretical transition densities show a rather strong dependence on the excitation energy.

PACS: 21.60.-n; 21.10.Re; 27.40.+z

1 Introduction

Electric giant resonances in double-magic nuclei have been studied for a long period of time, both experimentally and theoretically. In particular much attention has been paid to the "elder", *i.e.* isovector E1 resonance and to the oldest among the so-called new giant resonances discovered after 1971-72, namely , the isoscalar E0 and E2 resonances [1, 2, 3, 4]. However experimental data on isovector E0 and E2 resonances are rather scarce and much less systematic than for the isoscalar ones [2, 3, 4]. There are also many questions about isoscalar E0 resonances in nuclei with A < 90 [2, 3].

As for the nuclei where giant resonances studies have been performed, one of the most interesting areas for further investigations is that of the magic nuclei ^{40}Ca, ^{48}Ca and the unstable ^{56}Ni. There are many reasons for this, and we will enumerate some of them – mainly from the point of view of microscopic nuclear theory.

1. The most experimentally investigated nucleus is ^{40}Ca [2, 5, 6, 7, 8, 9] which is a bridge between the *sd* and *fp* nuclei. It has very noticeable specific properties: for example, a strong fragmentation of the isoscalar E0 and E2 resonances in the (10 - 20) MeV interval. It is caused by the 1p1h⊗phonon configurations [10, 11], which are more complex than those accounted for in the RPA, and also by strong ground state correlations (GSC) induced by these configurations [11].

The next magic nucleus, ^{48}Ca, was studied to a much lesser extent. It is very interesting to study the differences in properties, including that of GSC effects, between the LS-saturated nucleus ^{40}Ca and ^{48}Ca. However there are no detailed calculations for these nuclei within the same theoretical approach which would take into account all the necessary GSC. We will perform such calculations in this work.

There are no experimental data on giant resonances in unstable nuclei, including ^{56}Ni, and so far we have a small number of calculations for this nucleus (see for example the M1 and E0 resonance calculations [12, 13, 14]). In order to compare properties

of excitations in these three nuclei it is necessary to calculate them using the same approach. This is the first motivation of the present work, apart from the general interest at present in investigations of unstable nuclei [15].

2. It turned out that the microscopic approach which describes the above-mentioned fragmentation of the isoscalar E2 and E0 resonances must take into account not only RPA and more complex 1p1h⊗phonon configurations, but also the GSC caused by these complex configurations (GSC_{phon}). These correlations also play an important numerical, and sometimes principal, role in the description of the M1 strength in ^{40}Ca [16], isoscalar E0 strength in ^{40}Ca and ^{208}Pb [11, 14] and of other effects [17, 18].

The approach which describes these properties uses the parameters of the phenomenological non-separable interaction of the Landau- Migdal type. There are some theoretical justifications, which were confirmed by the calculations taking into account the RPA as well as 1p1h⊗phonon configurations in magic nuclei ^{16}O, ^{40}Ca, ^{48}Ca and ^{208}Pb, that these parameters are the same as those of the theory of finite Fermi systems (TFFS) of Migdal [19] and can be used for all nuclei except for light ones. That means that for ^{56}Ni the necessary parameters are already known and predictions of the ^{56}Ni properties should be reliable.

These features of the approach – to include the new dynamic GSC_{phon} effects and use the same for all the nuclei under consideration parameters – is the second motivation of the present calculations which employ the same approach as the above-mentioned calculations [11, 13, 14, 17, 18].

3. The approach under consideration includes, in addition to RPA configurations (which give an analog of the Landau damping in finite nuclei) and more complex 1p1h⊗phonon configurations (which give the fragmentation width $\Gamma\downarrow$), a coupling with the single-particle continuum which determines the escape width $\Gamma\uparrow$. The latter is rather important. Physically, this gives the realistic resonance envelope. Numerically this is also important because the contribution of the continuum for medium weight

nuclei should be more noticeable than that for heavy nuclei. This was confirmed by the E1 resonance calculations in Ref. [20] where the contribution of the continuum to the calculated total resonance width was 14% for ^{40}Ca, 28% for ^{48}Ca, and only 7% for ^{208}Pb.

Our approach is formulated from the very beginning for the density matrix in the coordinate representation. It is necessary to know the microscopic properties of the transition densities for the giant resonances and nuclei under considerations in order to use them in the calculations of various cross sections of the reactions where these resonances are excited, and also for comparison with the phenomenological transition densities often used in the analysis of experimental data. In addition, there are many questions and a discussion [9] about the microscopic transition density, *e.g.* about their dependence on the energy interval, coordinate, behaviour on the nuclear surface, and their form in various microscopic models.

These features of this approach, which are connected with explicit taking into account the single-particle continuum, are the third motivation for these calculations.

In this article, continuing our study in Ref. [11], we will calculate the E0, E1, E2 excitations in ^{40}Ca, ^{48}Ca, and ^{56}Ni which can be induced by electromagnetic probes. The isovector E1, isoscalar and isovector E0 and E2 as well as the usual (summary) electomagnetic E0 and E2 excitations will be investigated in a large energy interval. The latter is necessary to study the depletion of sum rules in the calculations and the influence of our GSC$_{phon}$ on the sum rules. It was observed that within the Extended Second RPA (ESRPA) [21] the GSC can change the linearly energy-weighted sum rules (EWSR). Therefore we first calculated these model independent, *i.e.* isovector E1, and almost model independent EWSR for the E0 and E2 excitations.

2 Theory

2.1 Initial quantities of the approach

The approach has been described in Ref. [20] and in much greater detail in Ref. [22].Here only our essential approximations and basic equations will be presented.

Our approach is a generalization of the TFFS to take explicitly into account, in addition to the RPA configurations, more complex 1p1h⊗phonon ones as well as the single-particle continuum. The initial input data of it are two sets of phenomenological parameters discribing the Woods-Saxon single-particle potential and the effective interaction of Landau-Migdal type. We do not use a connection between the mean field and the effective interaction because it is so far unknown, strictly speaking, for the configurations which are more complex than those accounted for in the RPA. As in the case of the standard TFFS, this means a non-selfconsistency of the approach.

In all of the approaches which include complex configurations in this way two questions concerning a double counting of the complex (in our case, 1p1h⊗phonon) configurations arise. It is necessary to extract the contribution of the complex configurations, which are treated explicitly, from the phenomenological quantities, *i.e.* from the mean field and from the effective interaction and local charges of quasiparticles. As far as the procedure for the mean field is concerned, this "refining" from our phonons is as follows. To obtain the new ("refined") single-particle basis $\{\tilde{\epsilon}_\lambda, \tilde{\varphi}_\lambda\}$ we must substract the contribution of the phonon mixing from the "old" phenomenological Woods-Saxon energies ϵ_λ:

$$\tilde{\epsilon}_\lambda = \epsilon_\lambda - M_{\lambda\lambda}(\epsilon_\lambda)$$
$$= \epsilon_\lambda - \frac{1}{2j+1}\sum_{s,\lambda\prime} |<\lambda \mid g_s \mid \lambda\prime>|^2 \{\frac{1-n_{\lambda\prime}}{\epsilon_\lambda - \tilde{\epsilon}_{\lambda\prime} - \omega_s} + \frac{n_{\lambda\prime}}{\epsilon_\lambda - \tilde{\epsilon}_{\lambda\prime} + \omega_s}\} \qquad (1)$$

where λ = {n, j, l}, and n_λ and g_s are single-particle occupation numbers and the creation phonon ampltudes.

In all our equations the new effective interaction $\bar{F}$ and local charges $\bar{e}_q$ enter and play the same role as the corresponding quantities F and e_q of the TFFS. By definition they should not contain the complex configurations which are considered explicitly and therefore, strictly speaking, the parameters describing $\bar{F}$ and $\bar{e}_q$ should be determined within the present approach from comparison with experiment. However we use a small number of collective and low-lying phonons, which give the main contribution to the giant resonances characteristics under consideration. The corrections of quantities F and e_q due to these phonons must be irregular and of a long-distance character. Therefore one hopes that these *non-local* corrections of the *local* quantities F and e_q are not important and that we can use the old parameters of F and e_q instead of the new ones. This approximation has been validated by our calculations [11, 13, 14, 20].

Thus, although the additional configurations, in contrast with the RPA or TFFS approach, are treated here explicitly, it is possible to obtain the initial quantities of our approach from the TFFS quantities. This means that practically all of the initial quantities are already known (see Sect.3) .

2.2 Basic equations

The basic equation of the approach is formulated in coordinate space for the transition density, which is the change of the density matrix in an external field V^0 with the energy ω:

$$\rho(\mathbf{r},\omega) = -\int A(\mathbf{r},\mathbf{r}',\omega)e_q V^0(\mathbf{r}')d^3r' - \int A(\mathbf{r},\mathbf{r}_1,\omega)F(\mathbf{r}_1,\mathbf{r}_2)\rho(\mathbf{r}_2,\omega)d^3r_1 d^3r_2 \ . \quad (2)$$

Here e_q and F are the local quasiparticle charge and the effective interaction. As discussed above they are taken from the TFFS, *e.g.*

$$F(\mathbf{r},\mathbf{r}') = C_0[f(r) + f'(r)\boldsymbol{\tau}_1\boldsymbol{\tau}_2 + (g + g'\boldsymbol{\tau}_1\boldsymbol{\tau}_2)\boldsymbol{\sigma}_1\boldsymbol{\sigma}_2]\delta(\mathbf{r}-\mathbf{r}'), \quad (3)$$

$$f(r) = f_{ex} + (f_{in} - f_{ex})\rho_0(r)/\rho_0(0),$$

where $\rho_0(r)$ is the nuclear density in the ground state.

In such a form Eq.(2) is quite similar to the usual RPA equation written in the coordinate representation for the transition density. All of the difference is contained in our generalized propagator A. It consists of two parts: the "refined" RPA and the part which contains much more complicated physics caused by 1p1h⊗phonon configurations. We use the following expression for the propagator A

$$A(\mathbf{r},\mathbf{r}',\omega) = \tilde{A}^{RPA}_{cont}(\mathbf{r},\mathbf{r}',\omega) + \sum_{1234}(A_{1234}(\omega) - \tilde{A}^{RPA}_{1234}(\omega)\delta_{13}\delta_{24})\tilde{\varphi}^*_1(\mathbf{r})\tilde{\varphi}_2(\mathbf{r})\tilde{\varphi}_3(\mathbf{r}')\tilde{\varphi}^*_4(\mathbf{r}') \ , \tag{4}$$

where $\tilde{A}^{RPA}_{cont}$ is the "refined" RPA propagator in which the single-particle continuum is taken into account exactly. The summation in eq.(4) is performed over two shells above and all shells below the Fermi level. Thus the single particle continuum is taken into account completely only in the RPA part of the propagator.

The expression for the propagator A_{1234} was obtained in the "refined" single-particle basis $(\tilde{\varphi}_\lambda, \tilde{\epsilon}_\lambda)$ in Ref. [23], see also Ref. [22]. It has rather cumbersome form which we do not write down here.

The excitation energies are determined by solving the system of homogeneous equations which are obtained from Eq.(1). The squared amplitudes of the transition from the ground to the excited states are given by the residues at the excitation energies of the polarizability operator,

$$\Pi(\omega) = \int d^3r[e_q V^0(\mathbf{r})]^* \rho(\mathbf{r},\omega). \tag{5}$$

It is often more convenient to deal with the strength function which gives the energy distribution of the excitation strength under consideration:

$$S(E,\eta) = \frac{dB(EL)}{dE} = -\frac{1}{\pi} Im\Pi(E + \imath\eta), \tag{6}$$

where η is a smearing parameter. In this way we take phenomenologically into account the complex configurations, which are not explicitly treated, and simulate a finite experimental resolution. Inclusion of a sufficiently large η also greatly reduces numerical difficulties in our calculations. Then the transition probability and the EWSR summed in the energy interval $[E_1, E_2]$ are given by

$$\sum_{[E_1,E_2]} B(EL) \uparrow = \frac{1}{2\pi i} \oint d\omega \Pi(\omega), \tag{7}$$

$$S_L = \sum_{[E_1,E_2]} E_i B_i(EL) \uparrow = \frac{1}{2\pi i} \oint d\omega \omega \Pi(\omega). \tag{8}$$

Here the integration contour in the complex energy plane intersects the real energy axis at the points E_1 and E_2.

2.3 Electric sum rules

We calculate only electromagnetically induced E0, E1 and E2 excitations. In order to avoid possible confusion we will define all the quantities here. The electric operators are

$$Q_{LM} = e \sum_{i=1}^{Z} r_i^L Y_{LM}(\Omega_i) \qquad\qquad L \geq 2, \tag{9}$$

$$Q_{00} = e \sum_{i=1}^{Z} r_i^2, \tag{10}$$

$$Q_{1M} = \frac{eN}{A} \sum_{i=1}^{Z} r_i Y_{1M}(\Omega_i) - \frac{eZ}{A} \sum_{i=1}^{N} r_i Y_{1M}(\Omega_i), \tag{11}$$

where the electric isovector dipole operator has the well-known kinematic charges $e_p = Ne/A$, $e_n = -Ze/A$. The corresponding electric full EWSR

$$S_L \equiv EWSR = \sum_k (E_k - E_0) B_k(EL) \uparrow$$

are given then by [24]

$$S_L = \frac{\hbar^2 e^2}{8\pi m_p} L(2L+1)^2 Z < r^{2L-2} >_p \qquad L \geq 2, \tag{12}$$

$$S_0 = \frac{2\hbar^2 e^2}{m_p} Z < r^2 >_p, \tag{13}$$

$$S_1 = \frac{9\hbar^2 e^2}{8m_p} \frac{NZ}{A}, \tag{14}$$

where the radial average is taken over the proton distribution in the ground state. The electric dipole EWSR (14) corresponds to the well-known Thomas-Reiche-Khun sum rules for photoabsorption cross section

$$\sigma_0^{cl} = \int \sigma(E) dE = \frac{2\pi^2 e^2 \hbar}{mc} \frac{NZ}{A}.$$

The sums S_2 and S_0 include both the isoscalar (ΔT = 0) and isovector (ΔT = 1) contributions. These contributions may be separated for the E0 and E2 transitions by means of the additional physical approximation $< \tau_3 >$ = (N - Z)/A [24] so that

$$Q_{LM} = Q^0_{LM} + Q^1_{LM},$$

where

$$Q^0_{LM} = \frac{eZ}{A} \sum_{i=1}^{A} r_i^L Y_{LM}(\Omega_i), \tag{15}$$

$$Q^1_{LM} = \frac{eN}{A} \sum_{i=1}^{Z} r_i^L Y_{LM}(\Omega_i) - \frac{eZ}{A} \sum_{i=1}^{N} r_i^L Y_{LM}(\Omega_i) \tag{16}$$

for $L \geq 2$ and

$$Q^0_{00} = \frac{eZ}{A} \sum_{i=1}^{A} r_i^2, \tag{17}$$

$$Q^1_{00} = \frac{eN}{A} \sum_{i=1}^{Z} r_i^2 - \frac{eZ}{A} \sum_{i=1}^{N} r_i^2 \tag{18}$$

for $L = 0$. The effective charges in Eqs.(16), (18) coincide with the kinematic charges for isovector E1 excitations, but they have another physical origin.

These operators give the following isoscalar and isovector electric EWSR's

$$S_L^0 = \frac{\hbar^2 e^2}{8\pi m_p} L(2L+1)^2 \frac{Z^2}{A} < r^{(2L-2)} >_p, \tag{19}$$

$$S_L^1 = \frac{\hbar^2 e^2}{8\pi m_p} L(2l+1)^2 \frac{ZN}{A} < r^{(2L-2)} >_p \tag{20}$$

for $L \geq 2$ [24] and

$$S_0^0 = \frac{2\hbar^2 e^2}{m_p} \frac{Z^2}{A} < r^2 >_p, \tag{21}$$

$$S_0^1 = \frac{2\hbar^2 e^2}{m_p} \frac{NZ}{A} < r^2 >_p \tag{22}$$

for $L = 0$.

We have calculated our strength distributions S(E) with the electric operators (9), (10), (11) for the full S(E), (15), (17) for the isoscalar S(E) and (16), (18) for the isovector S(E)

3 Numerical details

As discussed above, the Landau-Migdal interaction has been used both for giant resonances and for low-lying collective phonons which have been microscopically calculated within the standard TFFS [19]. In Eq.(3) we used the same set of the interaction parameters as in our previous calculations [11, 13, 14, 18, 20]

$$f_{in} = -0.002, f'_{ex} = 2.30, f'_{in} = 0.76, g = 0.05, g' = 0.96, C_0 = 300 MeV fm^3 \tag{23}$$

except for the parameter f_{ex}. Because of the non-selfconsistency of the approach, f_{ex} should be fitted so as to correctly obtain the energy of the spurious state 1^-. In these calculations as well as in Ref. [11] we used the calculated nuclear density in the ground state for $\rho_0(r)$

$$\rho_0(r) = \sum_{\epsilon_i \leq \epsilon_F} \frac{1}{4\pi}(2j_i+1)R_i^2(r). \tag{24}$$

where $R_i(r)$ are radial single-particle wave functions.

In our opinion such a choice of $\rho_0(r)$ instead of the usual Woods-Saxon form makes our calculations more consistent. For the medium-weight nuclei ^{40}Ca, ^{48}Ca, ^{56}Ni using Eq. (24) gives noticeably different results from those obtained using the Woods-Saxon form of $\rho_0(r)$ as compared with the difference for ^{208}Pb. Therefore we have obtained another value of f_{ex} = - 1.40. We have fitted the phonon energies by changing f_{ex} also; it turned out that for all three nuclei f_{ex} is in the interval (–1.73) – (–1.50).This numerical similarity to the previous value indirectly confirms the correctness of our method of choising f_{ex}.

The phonon characteristics,*i.e.* their energies and transition probabilities, which have been calculated microscopically within the standard TFFS [19], are given in Ref. [14]. We have included the following phonons: 3_1^-, 5_1^- in ^{40}Ca, 2_1^+, 3_1^- , 5_1^- in ^{48}Ca, and 2_1^+, 3_1^-, 5_1^-, 4_1^+ 6_1^+ in ^{56}Ni.

The single-particle levels and wave functions were calculated with the standard Woods-Saxon potential [25]. In order to get good agreement with the experimental single-particle energies, the well depth of the central part of the potential has been adjusted by changing the depth parameter by less than 5%. The single-particle energies thus obtained are given in Table 1.

Numerical values of all the EWSR's used in the calculations are presented in Table 2. The quantities $< r^2 >_p$ were obtained using the proton density distribution calculated from the above-described single-particle scheme for ^{40}Ca, ^{48}Ca, and ^{56}Ni.

The mean energies E_1, E_3, and dispersion D are determined by the following:

$$E_1 = \frac{p_1}{p_0}, \qquad E_3 = (\frac{p_3}{p_1})^{1/2}, \qquad D = \sqrt{\frac{p_2}{p_0} - (\frac{p_1}{p_0})^2} \tag{25}$$

where the energy momenta p_k corresponding to the enegy interval $\Delta E = E_{max} - E_{min}$ have been calculated as follows

$$p_k = \int_{E_{min}}^{E_{max}} dE E^k S(E) \tag{26}$$

We have also calculated the transition densities which are used in phenomenological and microscopic models and simply connected with our $\rho_L(r, E + \imath\eta)$ determined by Eq.(2):

$$\rho_L(r, \Delta E) = \frac{1}{\pi\sqrt{\Sigma B(EL)}} Im \int_{E_{min}}^{E_{max}} dE \rho_L(r, E + \imath\eta), \tag{27}$$

where $\Sigma B(EL)$ is the B(EL) value summed over the interval ΔE.

In all calculations here the smearing parameter $\eta = 500$ keV has been used.

4 Results and discussion

4.1 Photoabsorption cross sections and strength functions

The differences between the present and our earlier calculations are that: 1) here considerably larger energy intervals have been studied, and 2) we have made methodical changes in our numerical scheme by using another quantity ρ_0(r) in Eq. (3), as discussed in Sect. 3, and also by changing of two single-particle energies in ^{40}Ca, as discussed in Ref. [11]. The most noticeable consequences of these differences have been obtained for isoscalar E0 excitations; they will be discussed in Section 4.1.2

Results of our calculations for the energy distributions of E1 photoabsorption cross sections $\sigma(\omega)$ and strength functions S(ω) in large energy intervals are presented in Figs.1-3. The integral characteristics calculated for these intervals are given in Tables 3-5. The depletion of the corresponding EWSR's (in percentages) (14) in Table 3, (13), (21), (22) in Table 4 and (12), (19), (20) in Table 5 were obtained using the values of the reference EWSR's from Table 2. It is easy to obtain the absolute values of $\sum B(EL) \uparrow$ and EWSR using Eqs.(25) and Table 2.

The single-particle continuum was taken into account in all of the variants of the calculations in Figs. 1 - 5 and Tables 3 - 5 , namely the continuum RPA (which is

often called here as RPA), the continuum RPA + 1p1h$\otimes$ phonon configurations, and the continuum RPA + 1p1h$\otimes$phonon configurations + GSC_{phon}.

In all the calculations for large energy intervals which are given in Table 3-5 we have obtained 98% - 102% of the corresponding EWSR's for the RPA case as well as for the RPA + 1p1h$\otimes$configurations (without GSC_{phon}). However, taking into account our GSC_{phon}, which corresponds to "backwards going" diagrams with phonons, increases the EWSR's by 4% - 7% as a rule. This result is in accord with the analytically obtained result of Ref. [21] mentioned in the Introduction although our model and the ESRPA used in Ref. [21] differ greatly. The main differences are that we are using complex configurations with collective phonons while in the ESRPA "pure" 2p2h configurations are used and, in contrast to the ESRPA, we do not use perturbation theory in the effective interaction. The complex configurations in the ground state give rise to an increase of $< r^2 >_p$ and therefore of the EWSR, and it may be also change other ground state characteristics.

The role of GSC_{phon} is especially noticeable in the low-lying energy region. For the (5 - 12) MeV interval in ^{40}Ca we have 7% of our S_0^0 from Table 2 and 7.4% of S_2^0. The contribution of GSC_{phon} to these figures is 3.6% and 4.8%, respectively, *i.e.* more than half (for comparison, the contributions to this interval obtained whithin the RPA are 1.0% and 0.4%). There is also additional low-lying strength due to GSC_{phon} in ^{56}Ni (Figs. 2, 3); here it is 4.8% of S_0^0 in the (5.0 - 14.0) MeV interval as compared with 2.5% without GSC_{phon}, *i.e.* about half. For higher energies the role of GSC_{phon} is less; *e.g.* for the (10 - 20.5) MeV interval their contribution to the full E2 EWSR decreases it by about one fourth in ^{40}Ca.

4.1.1 E1 excitations

The comparison with experiment for isovector E1 resonances in ^{40}Ca and ^{48}Ca was made in our earlier work [20]. There theoretical curves were approximated with

lorentzians in the same energy interval where there are experimental points. Here we study considerably larger intervals. Comparing our results with experimental curves in Refs. [27] (^{40}Ca) and [26] (^{48}Ca), one can conclude that we have also obtained a good agreement with experiment for mean energies, total widths, and maximal values of photoabsorption cross sections. As we see from Fig.1, this agreement is mainly obtained by inclusion of 1p1h⊗phonon configurations but the role of our GSC_{phon} is noticeable at least for the E1 EWSR. * The results obtained with the continuum RPA are not able to describe experiment in ^{40}Ca and ^{48}Ca.

We have also calculated the depletion of EWSR in the experimetally studied intervals (10.0 - 32.0) MeV (σ_0^{exp} = 637.7 mbMeV) for ^{40}Ca and (11.0 - 27.5) MeV (σ_0^{exp} = 836.6 mbMeV) for ^{48}Ca and obtained 599.2 mbMeV (99.9% of σ_0^{cl}) and 635.3 mbMeV (90.8% of σ_0^{cl}), respectively.

4.1.2 E0 and E2 excitations

Due to changes in the numerical scheme mentioned at the beginning of this section, the isoscalar E0 resonance became more compact than in Ref. [14]. The main part of the resonance, *i.e.* 65% of S_0^0 from Table 2, is now in the (11.0 - 23.0) MeV interval (see Fig. 3). For comparison, in the (6.0 - 30.0) MeV interval we have 85.5%, whereas in Ref. [14] we had only 48.2% of our S_0^0. For this reason values of mean energies determined according to Eq.(25) for the large interval under consideration have changed noticeably.

However in these calculations one of the most interesting earlier results dealing with the role of GSC_{phon} in the low-lying energy region has been preserved (see the discussion just before Sect.4.1.1). In the (6.0 - 13.6) MeV interval in Ref. [14] there was 9.6% of our S_0^0 and we have 9.7% here.

*The results shown in Fig.1 and in Table 3 were obtained earlier with another set of parameters as compared with Eq.(23). Using the set (23) will not give a considerable numerical difference.

The comparison with experiment for isoscalar E0 and E2 excitations † in ^{40}Ca has been made in Ref. [11]. It was shown there that in order to explain the electron experiments [8], where both of the resonances are excited, it was necessary to take into account GSC_{phon} for both of them. This can be seen here from Fig.2 for the full electromagnetic E0 and E2 strengths in ^{40}Ca and also from Fig.3. A good description of the splitting of the isoscalar (E2+E0) strength into three peaks observed in Ref.[8] was obtained in [11]. The value of the (E2+E0)theoretical isoscalar EWSR in the observed interval (10.0 - 20.5) MeV, which is equal to [6581+(25/16π)3729] = 8436 e^2fm^4MeV, agrees with the experimental value (7899 $\pm$ 1580) e^2fm^4MeV. In Ref. [5] the contribution at (23.5 $\pm$ 4.7)% of the isoscalar E0 EWSR in the (10.5 - 15.7) MeV has been determined by two independent methods,*i.e.* in $(\alpha, \alpha\prime)$ and$(\alpha, \alpha\prime\alpha_0)$ reactions, as well as (30 $\pm$ 6)% in the (10.5 - 20.0) MeV interval only from $(\alpha, \alpha\prime)$ reactions. We have obtained good agreement with the experiment for the first interval — 20.7% of our S_0^0 in the (10.5 - 15.5) MeV region — and somewhat more in the second interval: 50.2% of S_0^0.

Recently new measurements of the isoscalar E0 resonance in ^{40}Ca have been performed in (α, α') experiments with E_α = 240 MeV at small angles including 0° [28]. The experiments were performed between (8 - 29) MeV of excitation energy. This allows a detailed comparison with theory because it includes the energy range of our previous [14] and present results. The experiment shows (92 $\pm$ 15)% of the isoscalar EWSR S_0^0 in this region. This is in an agreement with our recent results [11]. If one compares with our previous results [14], where we used a different residual interaction, one finds only 52% of the EWSR in the observed region [28]. The remaining part of

†In all our comparisons with experiments there is an uncertainty because in the experimental works, as a rule, there is no exact information about numerical values of the reference EWSR used. Therefore there may be a discrepancy due to the different value of $< r^2 >_p$ used here and in the experimental articles.

the isoscalar E0 strength was moved to higher energies.

It is well known that the E0 strength is very sensitive to the residual interaction. Due to above-mentioned change of the interpolation formula of the Landau-Migdal interaction, where the density dependence is calculated consistently with the mean field we obtained in the present approach a more compact isoscalar E0 resonance in ^{40}Ca (Fig.3) compared to the previous calculation [14]. In the intervals investigated by experiments we obtained theoretically 32% in the range (15 - 20) MeV and 82% of S_0^0 in the (8 - 29) MeV region compared to the experimental values of (33 $\pm$ 4)% and (92 $\pm$ 15)%, respectively. This also agrees with our analysis [11] of the $(e, e'x)$ experiments of Ref. [8].

For the mean energies of the isoscalar E0 resonance in ^{40}Ca we obtained the values of E_1^{th} = 18.4 MeV and E_3^{th} = 23.4 MeV (Table 4) whereas the experiment [28] gives E_1^{exp} = (18.89 $\pm$ 0.11) MeV and E_3^{exp} = (21.30 $\pm$ 0.12) MeV. The difference between theoretical and experimental values of E_3 is due to the different averaging intervals used which is especially important just for E_3. Our theoretical results agree not only in the integral characteristics. One can see a reasonable agreement between the gross structure of the isoscalar E0 strength function in Fig.3 and that of the cross section in Ref.[28]. The good agreement of the theoretical results with these experimental data supports our new theoretical treatment of the residual interaction.

A summary of the experimental data on the isoscalar E2 resonance in ^{40}Ca as well as detailed measurements of it have been made in Ref. [6]. The main conclusion of this analysis was that the full isoscalar E2 strength was located in the region(0 - 22) Mev and is divided in approximately equal parts around 13.5 Mev and 18 Mev. This splitting was confirmed later [2, 7, 8]. Our calculations have given 73.8% of S_2^0 from Table 2 for the (0 - 22) MeV region, 18.3% in the (12 - 15) MeV and 27.9% in the broader (10.5 - 16.5) MeV interval. For the (16.5 - 19.5) MeV and (15 - 21) MeV regions we have obtained 25% and 44.6%, respectively. Therefore it is difficult to

speak about the *equal* distribution between the regions around 13.5 Mev and 18 MeV, but the trend is the same and roughly corresponds to the experiment. The splitting can be seen in Fig.3. In agreement with the experiment in Ref. [8], we have obtained also the third maximum at 12 MeV.

As can be seen from Fig.3, the isovector E0 as well as isovector E2 resonances are spread out over larger regions than the corresponding isoscalar E0 and E2 resonances. There are also noticeable low-lying tails of isovector strength in the regions of isoscalar E0 and E2 resonances. Table 6 gives these results for all the nuclei under consideration. The total isovector E0+E2 contributions to the main region of the isoscalar E0 resonance are about one half for ^{40}Ca and ^{56}Ni and about one fourth for ^{48}Ca. These results may be important for electron scattering on these nuclei; at least a similar effect has been obtained in ^{28}Si$(e, e\prime\alpha)$ coincidence scattering [29]

4.2 Transition densities

In Fig.4 the isovector E1 transition densities calculated in our approach for the large energy interval are shown. There is no significant difference between the continuum RPA and our full calculations. In all cases there are maxima of proton and neutron transition densities on the nuclear surface with approximately equal amplitude and opposite signs. This corresponds to the isovector nature of these giant vibrations. We point out that the transition densities (27) are also large inside of the nucleus, especially for the protons in ^{48}Ca and for the neutrons in ^{56}Ni, which may be important in the analysis of (e, e') experiments carried out at large momentum transfer.

In order to understand better the dependence of $\rho(r)$ on the energy region, we have calculated it for the small energy intervals of 5 MeV (Fig.5). There is a considerable difference in the coordinate dependence as compared with the large interval as well as with the different intervals under consideration. Such a strong dependence on the energy region needs to be checked experimentally.

It is important to note that the three-node microscopic E0 transition densities ρ_{tr} for ^{56}Ni shown in Fig.5 are very different as compared with the phenomenological one-node ρ_{tr} used in the experimental data analysis [2]. Preliminary results of our analysis of the ^{56,58}Ni(α,α') reactions at E_α = 240 MeV show that the use of the phenomenological ρ_{tr} gives rise to much less E0 strength compared to our microscopic transition densities.

Recently new experiments for the isoscalar E0 resonance in ^{58}Ni have been published [30]. The main result of the experiments is that in the region (12 - 25) MeV less than 50% of the isoscalar E0 EWSR has been observed. Having in mind the good agreement between theory and experiment in ^{40}Ca discussed above, it is difficult to understand this result because, as we found nearly all the isoscalar E0 strength in ^{40}Ca, we can not imagine any mechanism which reduces the strength in heavier nuclei.

5 Conclusion

In this work the E1, E0, and E2 strength distributions have been calculated in large energy intervals for the spherical magic nuclei ^{40}Ca, ^{48}Ca and ^{56}Ni. Except for the RPA configurations and single-particle continuum, two additional ingredients, namely 1p1h$\otimes$phonon configurations and GSC$_{phon}$ induced by these configurations, have been included. In order to explain the available experimental data it was always necessary to take 1p1h$\otimes$phonon configurations into account. The role of the GSC$_{phon}$ is often important in the low-lying energy regions and, what is particulary interesting, they give an increase of all the EWSR's in all the nuclei of 4 - 7% as compared with the cases without them (where the full depletion of the EWSR's have been obtained).

A reasonable agreement with the newest experimental results for the isoscalar E0 resonance in ^{40}Ca has been obtained which confirms the interaction form used in Ref. [11] and here. This resonance has a more compact form in the present calculations

than in our previous ones [14], but it remaines strongly structured and spread out over a larger energy interval than the resonances in ^{48}Ca and ^{56}Ni. The same is true also for the isoscalar E2 resonance in ^{40}Ca. However, according to Table 6, these resonances in all the nuclei under consideration have EWSR depletions of roughly 70% in the broad ($>$ 10 MeV) regions for the isoscalar E0 and 75 - 80% in the regions of breadth greater than 13 MeV for the isoscalar E2 resonances. These broad distributions, including a nearly uniform isoscalar E2 distribution in the (12 - 22) MeV region, agree completely with the experiments on ^{40}Ca.

A noticeable contribution of the isovector strength has been obtained in the isoscalar E0 and E2 resonances regions.

The transition densities for the isovector E1 resonances have been calculated for two limiting cases: large energy regions and small ones. A strong dependence on the interval for the small one of 5 MeV has been obtained, and the role of complex 1p1h$\otimes$phonon configurations is essential here. In the calculations both for large energy regions and for small ones a considerable part of some density transitions is inside of the nucleus. It is desirable to study these features in a more detailed way both experimentally and theoretically. The latter is in progress now.

The work was partly supported by the German - Russian Scientific Exchange Program and Deutsche Forschungsgemeinschaft (contract 436RUS17/88/96). The authors are very thankful to Prof. D. Youngblood for useful discussions and communicating the experimental results [28] before publication , and to Prof. J. Durso for careful reading of the manusript.

References

[1] J. Speth, ed., Electric and magnetic giant resonances in nuclei (World Scientific, Singapore, 1991).

[2] A. van der Woude, in Ref.[1], p. 101.

[3] A. van der Woude, Nucl. Phys. A 599 (1996) 393c.

[4] M. Thoennessen, ed., Proc. Gull Lake Nucl. Physics Conf. on Giant Resonances, Nucl. Phys. A 569 (1994) Nos.1-2.

[5] S. Brandenburg, R. De Leo, A.G. Drentje, M.N. Harakeh, H. Sakai, and A.van der Woude, Phys. Lett. 130B (1983) 9.

[6] F. Zwartz, A.G. Drentje, M.N. Harakeh, and A. van der Woude, Nucl. Phys. A 439 (1985) 117.

[7] J. Lisantti, D.J. Horen, F.E. Bertrand, R.L. Auble, B.L. Burke, E.E. Gross, R.O. Sayer, D.K. McDaniels, K.W. Jones, J.B. McClelland, S.J. Seestrom-Morris, and L.W. Swenson, Phys. Rev. C 40 (1989) 211.

[8] H. Diesener, U. Helm, G. Herbert, V. Huck, P. von Neumann-Cosel, C. Rangacharyulu, A. Richter, G. Schrieder, A. Stascheck. A Stiller, J. Ryckebusch, and J. Carter, Phys. Rev. Lett. 72 (1994) 1994.

[9] H. Diesener, U. Helm, P. von Neumann-Cosel, A Richter, G. Schrieder, and S. Strauch, Phys. Lett. B 352 (1995) 201.

[10] P.F. Bortignon and R.A. Broglia, Nucl. Phys. A 371 (1981) 405.

[11] S. Kamerdzhiev, J. Speth, and G. Tertychny, Phys. Rev. Lett. 74 (1995) 3943.

[12] E. Migli, S. Drożdż, J. Speth, and J. Wambach, Z. Phys. 340 (1991) 111.

[13] S. Kamerdzhiev, J. Speth, G. Tertychny, and J. Wambach, Z. Phys. A 346 (1993) 253.

[14] S. Kamerdzhiev, J. Speth, G. Tertychny, and J. Wambach, Nucl. Phys. A 577 (1994) 641.

[15] H. Horiuchi, K. Ikeda, K. Sato, Y. Suzuki, and I. Tanihata, eds., Nucl. Phys. A 588 (1995) No.1;
R. Wyss, ed., Physica Scripta 56 (1995).

[16] S.P. Kamerdzhiev and V.N. Tkachev, Phys. Lett. B 142 (1984) 225; Z. Phys. A 334 (1989) 19.

[17] S. Kamerdzhiev and J. Speth, Nucl. Phys. A 599 (1996) 373c.

[18] S.Kamerdzhiev, J. Speth, and G. Tertychny, Nucl. Phys. A 569 (1994) 313c.

[19] A.B. Migdal, Theory of finite Fermi systems and applications to atomic nuclei (Wiley, New York, 1967).

[20] S.Kamerdzhiev, J. Speth, G. Tertychny, and V. Tselayev, Nucl. Phys. A 555 (1993) 90.

[21] S. Adachi and E.L. Lipparini, Nucl. Phys. A489 (1988) 445.

[22] S.P. Kamerdzhiev, G.Ya. Tertychny, and V.I. Tselyaev, submitted to Fiz. Elem. Chastits At. Yadra.

[23] V.I.Tselayev, Sov. J. Nucl. Phys. A489 (1988) 445.

[24] E.K. Warburton and J. Weneser, Isospin in nuclear physics, ed. D.H. Wilkinson (North-Holland, Amsterdam, 1969) p. 173.

[25] V.A. Chepurnov, Sov. J. Nucl. Phys. 6 (1967) 696.

[26] G.J. O'Keefe, M.N. Thompson, Y.I. Assafiri, R.E. Pywell, and K. Shoda, Nucl.Phys. A469 (1987) 239.

[27] J. Ahrens, H. Borchert, K.H. Czock, H.B. Eppler, H. Gimm, H.Gundrum, M. Krönig, P. Riehn, G. Sita Ram, A. Ziegler, and B. Ziegler, Nucl. Phys. A251 (1975) 479.

[28] D.H. Youngblood, Y.-W. Lui, H.L. Clark, Submitted to Phys. Rev. C

[29] Th. Khim, K.T. Knöpfle, H. Riedesel, P. Voruganti, H.J. Emrich, G. Fricke, R. Neuhausen, and R.K.M. Schneider, Phys. Rev. Lett. 56 (1986) 2789.

[30] D.H. Youngblood, H.L. Clark, and Y.-W. Lui, Phys. Rev. Lett. 76 (1996) 1429.

Figure captions

Fig.1. The calculated isovector E1 photoabsorption cross section for ^{40}Ca and ^{48}Ca and E1 strength function for ^{56}Ni. The final results are shown by the solid curve. The RPA + 1p1h$\otimes$phonon (without GSC_{phon}) and the continuum RPA results are shown by the dashed and dotted curves, respectively.

Fig.2. The full E0 and E2 electromagnetic strength functions calculated in the (5.0 - 45.0) MeV interval. The legend is the same as in Fig.1.

Fig.3. The full, isoscalar and isovector E0 and E2 strength functions calculated with taking into account RPA and 1p1h$\otimes$phonon configurations, the single- particle continuum and GSC_{phon}.

Fig.4. The isovector E1 transition densities calculated for the large energy interval (10 - 55) MeV in ^{40}Ca, (10 - 35) MeV in ^{48}Ca and (5 - 45) MeV in ^{56}Ni. For ^{40}Ca and ^{48}Ca the continuum RPA results are also shown.

Fig.5. The isovector E1, isoscalar E0 and isoscalar E2 transition densities in ^{56}Ni for the 5 MeV interval in the various parts of energy spectrum.

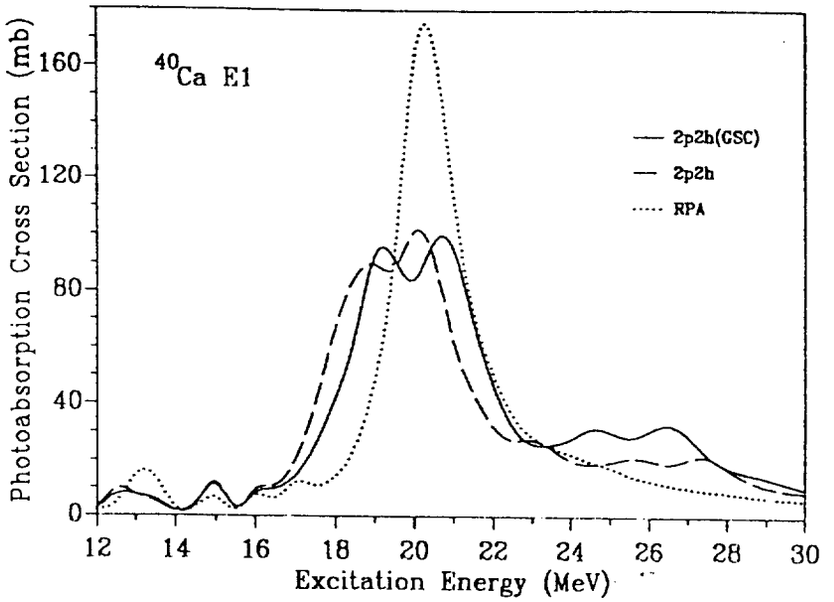
^{40}Ca E1
2p2h(GSC)
2p2h
RPA
Photoabsorption Cross Section (mb)
Excitation Energy (MeV)

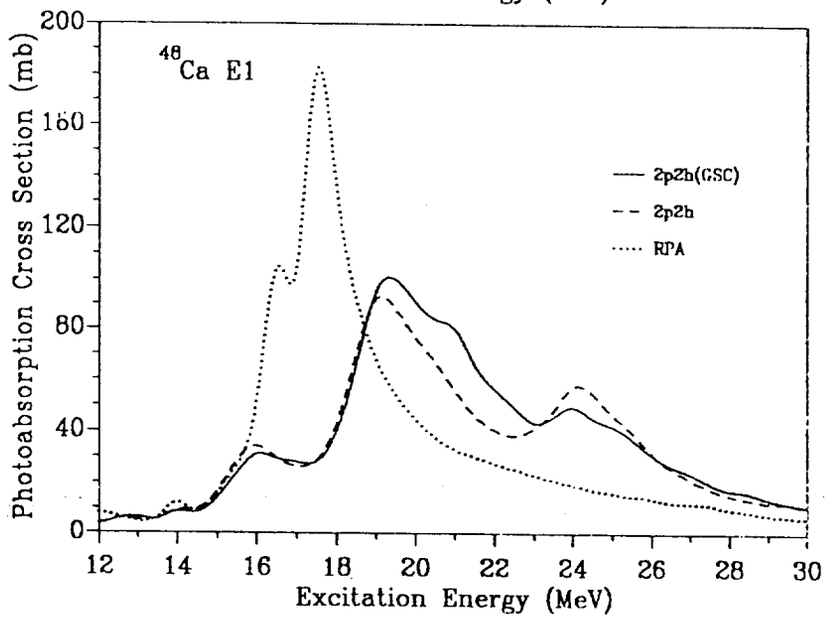
^{48}Ca E1
2p2h(GSC)
2p2h
RPA
Photoabsorption Cross Section (mb)
Excitation Energy (MeV)

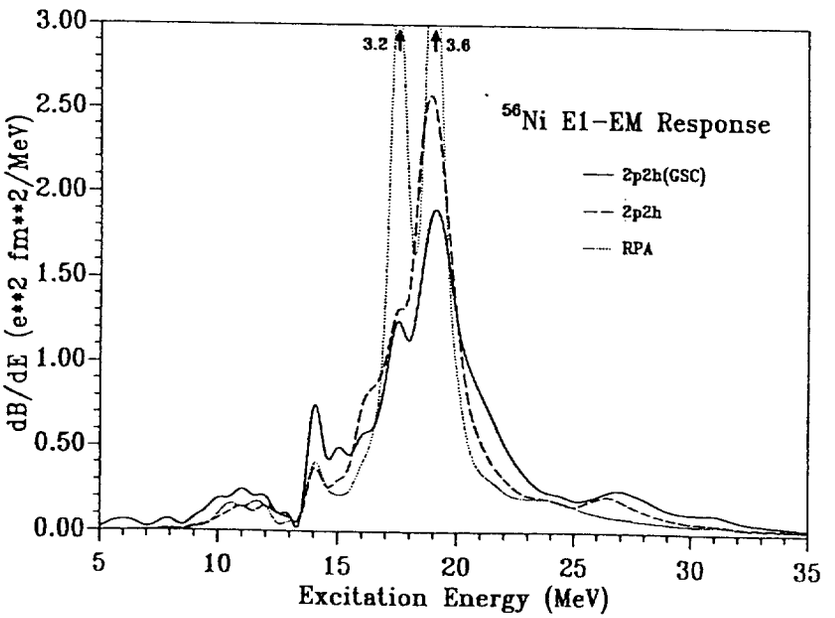
3.2
3.6
^{56}Ni E1-EM Response
2p2h(GSC)
2p2h
RPA
dB/dE (e**2 fm**2/MeV)
Excitation Energy (MeV)

Fig. 1

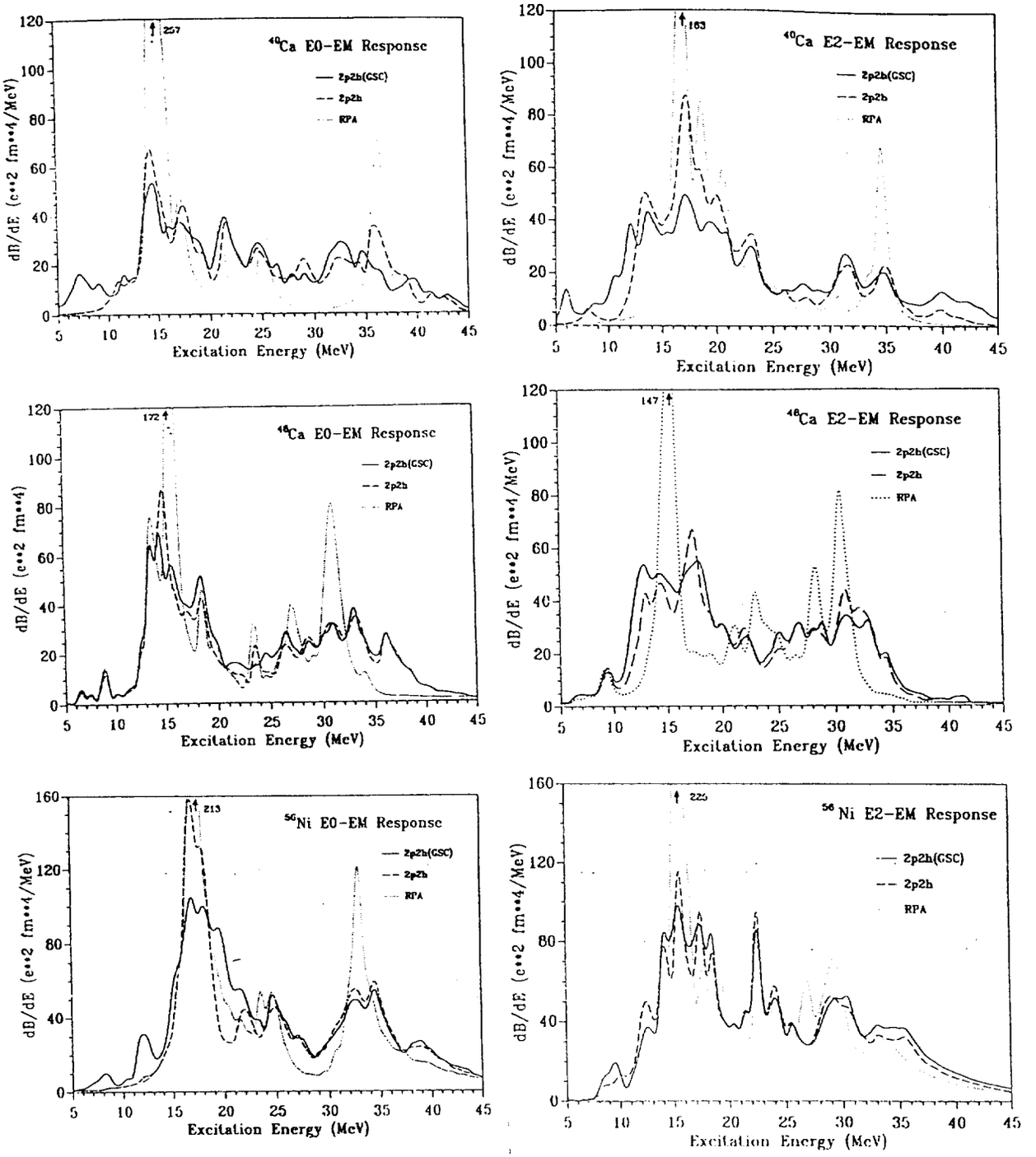
40Ca E0-EM Response
40Ca E2-EM Response
46Ca E0-EM Response
46Ca E2-EM Response
56Ni E0-EM Response
56Ni E2-EM Response
2p2h(GSC)
2p2h
RPA
dB/dE (e**2 fm**4/MeV)
Excitation Energy (MeV)
257
163
172
147
213
225

Fig. 2

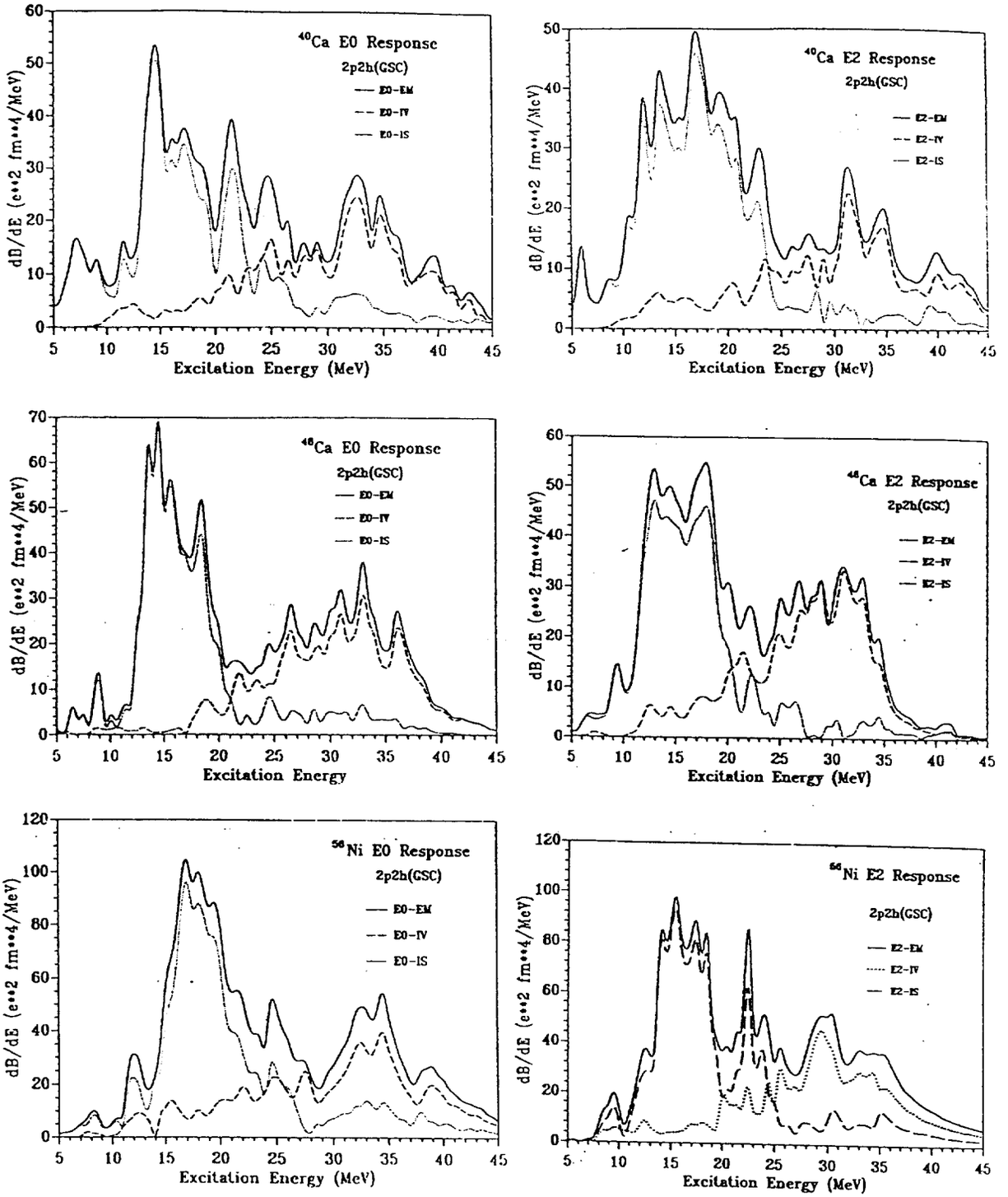
^{40}Ca E0 Response
2p2h(GSC)
E0-EM
E0-IV
E0-IS
dB/dE (e**2 fm**4/MeV)
Excitation Energy (MeV)
^{40}Ca E2 Response
2p2h(GSC)
E2-EM
E2-IV
E2-IS
dB/dE (e**2 fm**4/MeV)
Excitation Energy (MeV)
^{48}Ca E0 Response
2p2h(GSC)
E0-EM
E0-IV
E0-IS
dB/dE (e**2 fm**4/MeV)
Excitation Energy
^{48}Ca E2 Response
2p2h(GSC)
E2-EM
E2-IV
E2-IS
dB/dE (e**2 fm**4/MeV)
Excitation Energy (MeV)
^{56}Ni E0 Response
2p2h(GSC)
E0-EM
E0-IV
E0-IS
dB/dE (e**2 fm**4/MeV)
Excitation Energy (MeV)
^{56}Ni E2 Response
2p2h(GSC)
E2-EM
E2-IV
E2-IS
dB/dE (e**2 fm**4/MeV)
Excitation Energy (MeV)

Fig. 3

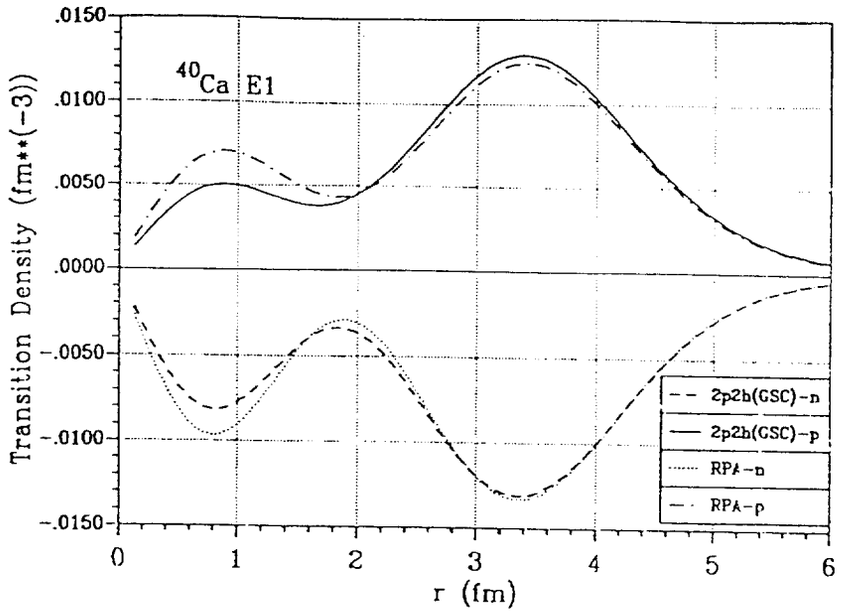
^{40}Ca E1
Transition Density (fm**(-3))
r (fm)
2p2h(GSC)-n
2p2h(GSC)-p
RPA-n
RPA-p

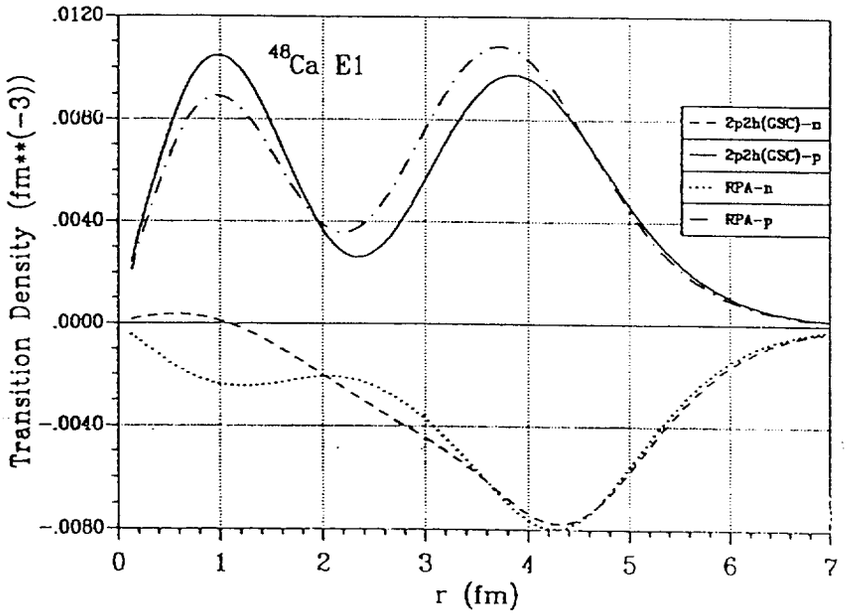
^{48}Ca E1
Transition Density (fm**(-3))
r (fm)
2p2h(GSC)-n
2p2h(GSC)-p
RPA-n
RPA-p

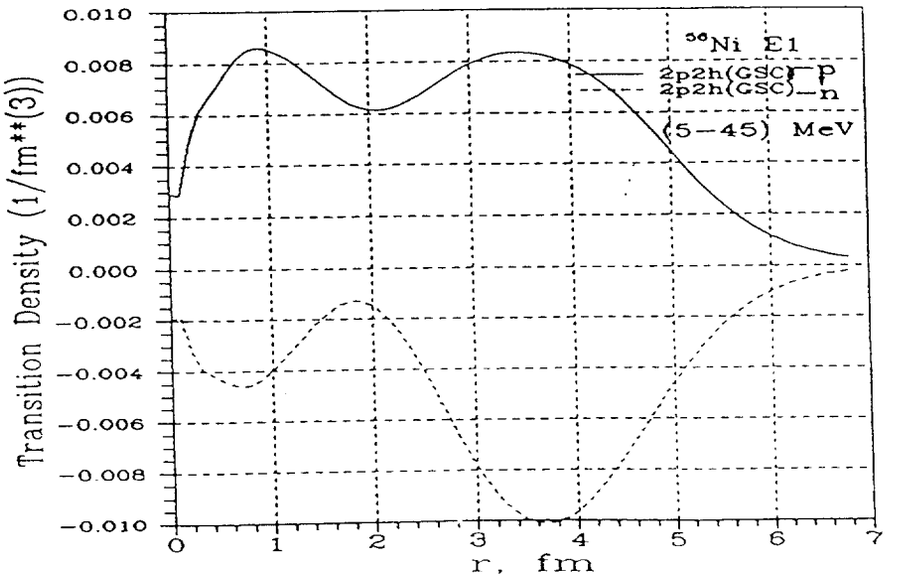
^{56}Ni E1
2p2h(GSC)-p
2p2h(GSC)-n
(5-45) MeV
Transition Density (1/fm**(3))
r, fm

Fig. 4

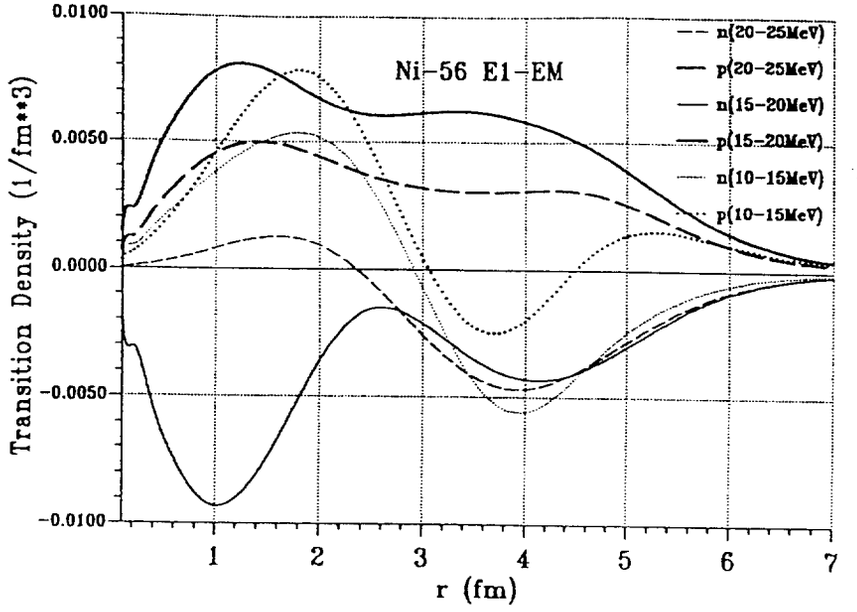
Ni-56 E1-EM
Transition Density (1/fm**3)
r (fm)
n(20-25MeV)
p(20-25MeV)
n(15-20MeV)
p(15-20MeV)
n(10-15MeV)
p(10-15MeV)

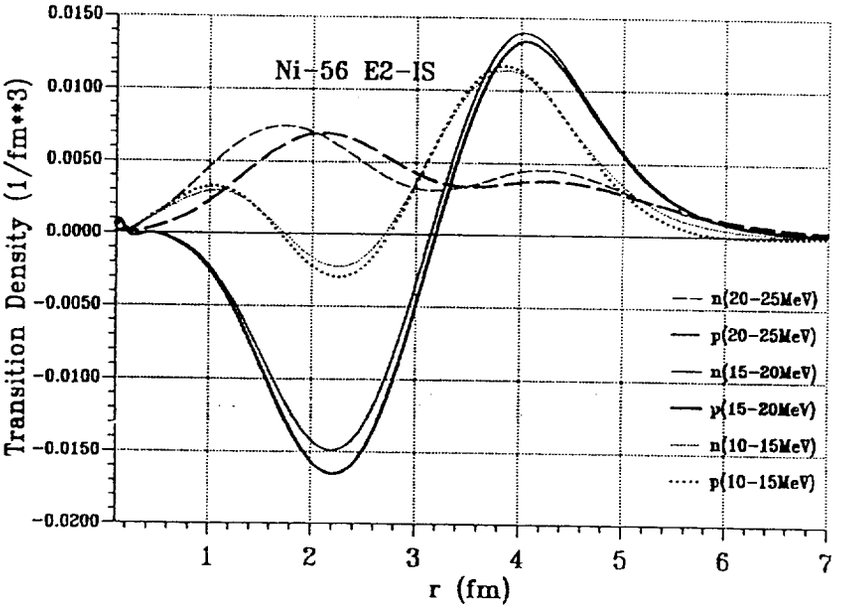
Ni-56 E2-IS
Transition Density (1/fm**3)
r (fm)
n(20-25MeV)
p(20-25MeV)
n(15-20MeV)
p(15-20MeV)
n(10-15MeV)
p(10-15MeV)

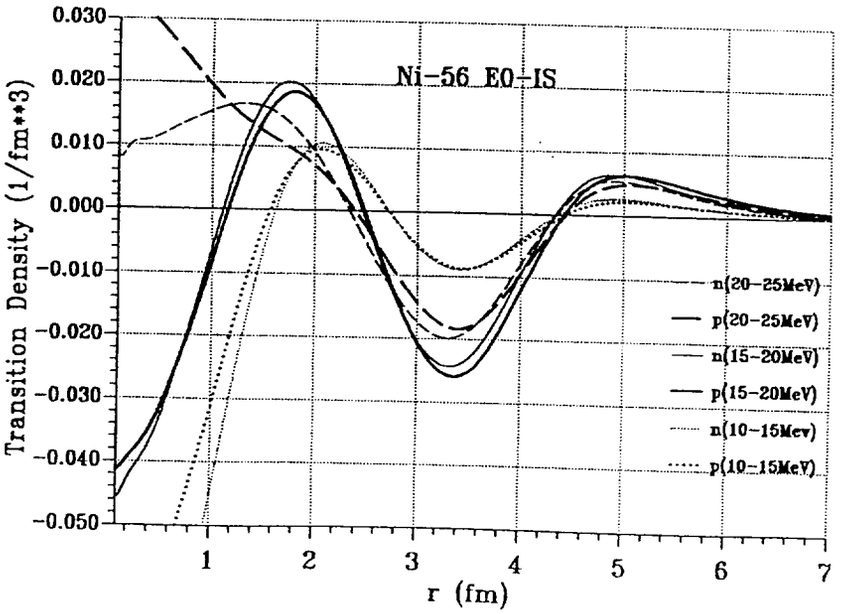
Ni-56 E0-IS
Transition Density (1/fm**3)
r (fm)
n(20-25MeV)
p(20-25MeV)
n(15-20MeV)
p(15-20MeV)
n(10-15Mev)
p(10-15MeV)

Fig. 5

Table 1. The single-particle levels used in the calculations.

nl_j	^{40}Ca		^{48}Ca		^{56}Ni	
	n	*p*	*n*	*p*	*n*	*p*
$1s_{1/2}$	-45.61	-37.39	-32.40	-37.18	-44.34	-37.19
$1p_{3/2}$	-33.65	-24.97	-26.57	-29.70	-33.68	-26.12
$1p_{1/2}$	-30.84	-22.12	-24.89	-28.54	-32.99	-24.39
$1d_{5/2}$	-21.80	-14.66	-17.84	-21.20	-27.29	-20.74
$2s_{1/2}$	-18.14	-10.83	-12.59	-15.80	-22.79	-15.98
$1d_{3/2}$	-15.64	-8.26	-12.51	-16.17	-21.33	-14.73
$1f_{7/2}$	-8.35	-1.29	-9.90	-9.61	-16.83	-7.92
$2p_{3/2}$	-6.44	0.56	-5.14	-6.51	-10.69	-3.58
$1f_{5/2}$	-2.72	4.78	-1.15	-4.55	-10.04	-1.08
$2p_{1/2}$	-4.29	2.30	-3.09	-5.06	-9.80	-2.06
$1g_{9/2}$	3.69	8.99	-0.73	-0.57	-7.51	-0.02
$2d_{5/2}$	1.55	8.09	1.75	1.77	-3,20	2.95
$3s_{1/2}$	8.49	5.66	1.02	2.73	-2.12	3.85
$2d_{3/2}$	4.35	12.13	5.32	4.59	-0.11	5.85

Table 2. Values of the reference EWSR's (14),(13),(21),(22),(12),(19),(20) for ^{40}Ca, ^{48}Ca, ^{56}Ni. The quantities σ_0^{cl} and S_1 for isovector E1 excitations are given in MeV mbarn and e^2MeV fm^2, respectively; the rest of the quantities are given in e^2MeV fm^4.

Nucleus		^{40}Ca	^{48}Ca	^{56}Ni
E1	$\sigma_0^{cl} = 60 \cdot \frac{NZ}{A}$	600	700	840
	$S_1 = 14.86 \cdot \frac{NZ}{A}$	148.6	173.4	208.0
E0	$S_0 = 83.0 \cdot Z < r^2 >_p$	16500	17921	31682
	$S_0^0 = 83.0 \cdot \frac{Z^2}{A} < r^2 >_p$	8250	7467	15841
	$S_0^1 = 83.0 \cdot \frac{NZ}{A} < r^2 >_p$	8250	10454	15841
E2	$S_2 = 82.55 \cdot Z < r^2 >_p$	16412	17827	31514
	$S_2^0 = 82.55 \cdot \frac{Z^2}{A} < r^2 >_p$	8206	7428	15757
	$S_2^1 = 82.55 \cdot \frac{NZ}{A} < r^2 >_p$	8206	10399	15757

Table 3. Integral characteristics of isovector E1 excitations in ^{40}Ca, ^{48}Ca and ^{56}Ni. The values of σ_0^{cl} are given in Table 2, the mean energies E_1 and E_3 and dispersions in MeV (for definition see Eq.(25)).

1^-	^{40}Ca (10-55) MeV				^{48}Ca (10-35) MeV				^{56}Ni (5-45) MeV			
	% σ_0^{cl}	E_1	E_3	D	% σ_0^{cl}	E_1	E_3	D	% σ_0^{cl}	E_1	E_3	D
RPA	98.0	21.2	22.9	4.7	96.7	18.6	19.9	4.0	100.9	18.9	20.3	3.6
RPA+1p1h⊗phonon	100.0	21.1	23.1	5.1	96.7	20.5	22.0	4.6	101.4	19.4	20.9	4.1
RPA+1p1h⊗phonon+GSCphon	109.2	21.8	24.0	5.4	103.9	20.7	22.1	4.6	104.9	19.5	21.8	4.5

Table 4. Integral characteristics of E0 excitations in ^{40}Ca, ^{48}Ca and ^{56}Ni calculated for the large energy region (5.0-45.0) MeV. The reference EWSR's are given in Table 1, the mean energies E_1 and E_3 in MeV.

0^+		^{40}Ca			^{48}Ca			^{56}Ni		
		% EWSR	E_1	E_3	% EWSR	E_1	E_3	% EWSR	E_1	E_3
RPA	(IS+IV)	101.0	20.5	26.0	100.7	21.3	25.2	101.1	24.2	28.3
RPA+1p1h⊗phonon	(IS+IV)	101.7	23.9	28.8	101.2	23.3	28.1	101.4	25.1	29.3
RPA +	(IS+IV)	106.4	23.0	28.4	106.2	23.3	28.0	106.7	24.4	28.9
1p1h ⊗ phonon +	IS	106.7	18.4	23.2	105.0	17.7	24.0	105.2	20.8	24.7
GSCphon	IV	105.0	29.8	32.5	104.0	30.0	32.0	103.5	29.4	32.5

Table 5. Integral characteristics of E2 excitations in ^{40}Ca, ^{48}Ca and ^{56}Ni calculated for the large energy region (5.0-45.0) MeV. The reference EWSR's are given in Table 2, the mean energies E_1 in MeV.

2^+		^{40}Ca		^{48}Ca		^{56}Ni	
		% EWSR	E_1	% EWSR	E_1	% EWSR	E_1
RPA	(IS+IV)	101.0	21.8	98.4	21.6	99.8	22.7
RPA+1p1h⊗phonon	(IS+IV)	101.0	21.3	99.5	22.1	100.2	23.2
RPA + 1p1h ⊗ phonon + +GSCphon	(IS+IV)	106.0	22.3	104.2	21.6	105.1	23.6
	IV	101.3	29.4	103.0	27.1	104.1	28.8
	IS	106.6	17.9	104.5	16.9	104.8	20.0

Table 6. Contributions of the isoscalar (fourth line) and isovector (fifth line) strength to the main regions of the isoscalar E0 and isoscalar E2 resonances (in percentages of EWSR's from Table 2).

Nucleus	^{40}Ca		^{48}Ca		^{56}Ni	
Isoscalar resonances	E0	E2	E0	E2	E0	E2
Interval, MeV	11-23	9-25	11-21	9-21	11-25	9-25
% IS EWSR	65.0	83.6	73.3	77.2	70.1	74.2
% IV EWSR	10.8	16.6	4.2	10.4	18.9	17.7